NANOSYSTEMS:
PHYSICS, CHEMISTRY, MATHEMATICS

Martinson K.D., et al. *Nanosystems: Phys. Chem. Math.*, 2025, **16** (4), 483–490.
http://nanojournal.ifmo.ru
DOI 10.17586/2220-8054-2025-16-4-483-490

Original article

Electrochemical characteristics of copper oxide nanoparticles synthesized by solution combustion method with controlled morphology

Kirill D. Martinson[1], Angelina O. Lebed[2], Hermann E. Litosov[3], Maria V. Kaneva[1], Artem A. Lobinsky[1]

[1]Ioffe Institute, St. Petersburg, Russia

[2]St. Petersburg Electrotechnical University "Leti", St. Petersburg, Russia

[3]St. Petersburg State Institute of Technology, St. Petersburg, Russia

Corresponding author: Kirill D. Martinson, martinsonkirill@mail.ru

PACS 61.05.C, 61.82.Rx, 65.40.gk

ABSTRACT Copper oxide (CuO) nanoparticles were obtained under solution combustion conditions using glycine as an organic fuel and a chelating agent at different redox ratios ($f = 0.2$, 1.0, and 1.6). The obtained powders were thermally treated at 300 °C for 30 min and characterized by Thermogravimetry differential thermal analysis (DTA/TG), scanning electron microscopy (SEM), energy-dispersive spectroscopy (EDS), powder X-ray diffraction (XRD), and atomic absorption spectrometry (AAS). The electrochemical characteristics were determined by cyclic voltammetry (CV), galvanostatic charge-discharge (GCD) and electrochemical impedance spectroscopy (EIS). The average crystallite sizes and specific surface areas of the obtained samples varied in the range from 4.8 to 18.6 nm and 14.4 to 78.4 m^2/g. The largest specific surface area corresponds to the sample synthesized at $f = 0.2$, which also has the smallest particle size (4.8 nm). The electrochemical behavior of copper oxide nanopowders depends significantly on structural and morphological features. The excellent specific capacity of the microstructure of the CuO sample synthesized at a significant fuel deficiency ($f = 0.2$) is explained by its large surface area and large pore radius.

KEYWORDS solution combustion synthesis, copper oxide, nanoparticles, electrochemistry characteristics

ACKNOWLEDGEMENTS The authors of the article express their gratitude to the Institute of Applied Materials Science of the Joint-Stock Company "Almaz Antej – Obuhovskij zavod" for assistance in conducting the study of morphology and structure. This work was funded by Russian Science Foundation (grant number 24-19-20060, https://rscf.ru/project/24-19-20060/) and St. Petersburg Science Foundation (agreement number 24-19-20060).

FOR CITATION Martinson K.D., Lebed A.O., Litosov H.E., Kaneva M.V., Lobinsky A.A. Electrochemical characteristics of copper oxide nanoparticles synthesized by solution combustion method with controlled morphology. *Nanosystems: Phys. Chem. Math.*, 2025, **16** (4), 483–490.

1. Introduction

Transition metal oxides are an important object of research for many scientific groups worldwide due to the variety of their practical applications, such as biomedicine, catalysis, coatings, electrochemistry, biosensors, pharmaceuticals and many other fields [1–3]. Among the variety of transition metal oxides, copper oxide (CuO) stands out in particular, being an important compound due to its set of unique physical, chemical and electrochemical properties [4]. Copper (II) oxide has outstanding semiconductor properties, which allows it to be actively used in the production of materials for electronics [5]. In addition, copper oxide is actively used in the production of photovoltaic devices, gas sensors, transistors and diodes [6], as catalysts and photocatalysts [7], antibacterial materials [8] and in lithium-ion batteries and supercapacitors [9].

The functional properties of copper oxide are largely determined by its structure. The crystal structure is monoclinic, in which each copper atom is surrounded by four oxygen atoms located at the vertices [10]. The copper atoms are located in the center of octahedra consisting of six oxygen atoms. The octahedra are distorted due to differences in the lengths of the Cu–O bonds: four shorter bonds lie in a plane, forming a "flat square", and two longer bonds are located perpendicular to this plane. Copper (II) oxide is a typical semiconductor with a narrow band gap in the range from 1.2 to 1.7 eV [11]. The narrow band gap allows CuO to absorb light in the visible range, which makes it suitable for use in photocatalysis and solar energy. High theoretical specific capacity, low cost and abundance in nature provide CuO with key advantages in the production of lithium-ion batteries and supercapacitors. The ability of ions to intercalate from the solution into the active material is contingent upon the electrode material's structure. Specifically, a higher surface area and porous architecture enhance the utilization of the electrode material, allowing sufficient time for both charging and discharging, which ultimately results in higher specific capacitance [12, 13]. Nanostructured materials demonstrate

improved charge-discharge rate due to larger specific surface volume and improved ionic conductivity. CuO is capable of rapid surface oxidation-reduction, which provides high capacity due to pseudocapacitative processes. In addition, copper (II) oxide demonstrates high values of specific capacity due to its ability to multiple oxidation-reduction reactions [14]. It should be noted that copper oxide is a more economically advantageous material in terms of its cost compared to noble metals. Obtaining CuO in the form of nanofilms, nanowires, nanoparticles and other nanostructures increases the effective surface area and improves interaction with the electrolyte. Combining CuO with conductive materials (graphene, carbon nanotubes) also increases conductivity and electron transfer rate [15].

There are many works devoted to the production of copper oxide nanoparticles using various wet chemistry methods. The most popular methods include hydrothermal synthesis, coprecipitation method, solution combustion method and various types of electrochemical methods [16–18]. Control of the parameters of copper oxide production methods allows one to significantly change the morphological features, dimensional parameters and physicochemical properties, which is important for optimizing its functionality in specific areas of application [19]. Special mention should be made of the types of solution combustion method, which in recent years have gained popularity as an effective and simple method for producing copper oxide nanopowders [20]. Due to the possibility of implementing the processes of nanoparticle formation under conditions of limited mass transfer using combustion methods, it is possible to control the morphology, structure and, as a consequence, the functional properties of materials in wide ranges of values [21]. For example, in [17] the photocatalytic and antimicrobial properties of 11 nm CuO nanorods synthesized by the direct solution combustion method using citric acid as an organic fuel were studied. In [22], the direct solution combustion method with citric acid was also used to obtain copper oxide nanoparticles with an average size of about 20 – 24 nm at different redox ratios. In addition, a thermogravimetry differential thermal analysis was performed which showed that the copper oxide formation temperature was in the range of 250 – 270 °C. In the article [23], Cheng H.-H. and his team obtained copper oxide nanoparticles using glycine as a fuel, however, all synthesized samples contained a mixture of phases consisting of CuO and Cu_2O oxides and metallic copper. In addition, the average particle size was in the range from 76.3 to 99.4 nm. Thus, despite the abundance of literary data that touched on the issues of obtaining CuO nanoparticles under solution combustion conditions, the question of the influence of oxidation-reduction ratios on the morphological features and structural and electrochemical parameters of copper oxide still remains not fully understood.

This work is devoted to the issues of synthesis of copper oxide nanoparticles by the method of solution combustion using glycine as an organic fuel. The main novelty of the work is the synthesis of nanoparticles under conditions of significant excess, deficiency and stoichiometry of fuel, the search for the relationship between the morphology of the obtained powders with their surface characteristics and electrochemical parameters.

2. Experimental

The following reagents were used to synthesize the initial powders: cupper nitrate ($Cu(NO_3)_2{\cdot}3H_2O$, puriss., NevaReactiv), glycine (CH_2NH_2COOH, puriss., NevaReactiv), nitric acid (HNO_3, puriss., NevaReactiv), and distilled water. A 5 M solution of HNO_3 and copper nitrate were added to the distilled water under constant mechanical stirring. Then glycine was added in various ratios f (0.2, 1.0, and 1.6, where 1.0 is the stoichiometric ratio of glycine according to the formation reaction) [24]. The solution obtained in this way was heated on a ceramic plate until the water was completely removed and the autoignition point was reached. Nitric acid was used to prevent the formation of impurity complex compounds of copper and glycine. After reaching the self-ignition point, gaseous combustion products (N_2, NO, NO_2, CO, CO_2) and copper oxide in the form of a brown powder were formed. The solid product obtained in this way was mechanically ground in a mortar and thermally treated at a temperature of 300 °C for 30 minutes to remove unreacted organic compounds. After thermal treatment, the powder was re-ground and analyzed using a set of physical and chemical methods.

Thermogravimetry differential thermal analysis was performed using a Shimadzu DTG-60 instrument (DTA/TG mode). Completely X-ray amorphous powder ($f = 0.05$) was analyzed in air atmosphere in the temperature range from 30 to 800 °C, with a heating rate of 10 °C/minute. The morphology of the synthesized powders was determined using the scanning electron microscopy method using a Tescan Vega 3 SBH scanning electron microscope. The elemental composition of the composites was analyzed by energy-dispersive spectroscopy using an Oxford INCA attachment. X-ray phase and X-ray structural analysis were performed on the basis of diffraction patterns obtained by powder X-ray diffractometry using a Rigaku SmartLab 3 diffractometer with CuKα_1 radiation ($\lambda = 0.154056$ nm) at 40 kV and 30 mA. Diffraction patterns were collected over a 2θ range of 20° to 80°, with a step size of 0.01° and a 3-second exposure time per step. The crystallite size was determined by the Williamson-Hall method, and the crystallite distribution was obtained using the fundamental parameters method. The unit cell parameters, degree of crystallinity and lattice microstrains were analyzed using Rigaku SmartLab Studio II software. Using the low-temperature nitrogen (N_2) sorption-desorption method, the specific surface area of the samples was determined using a micromeritics ASAP 2020 device. Sample preparation consisted of preliminary degassing in a vacuum at a temperature of 300 °C for 4 hours. The specific surface area values were calculated using the Brunauer–Emmett–Teller (BET) equation.

The electrochemical characteristics were determined using potentiostat Elins P-45X with three-electrode electrochemical cell. Measurements were performed by cyclic voltammetry (CV), galvanostatic charge-discharge (GCD) and

electrochemical impedance spectroscopy (EIS) techniques in a 1 M KOH aqueous electrolyte. The working electrode was obtained by deposition suspension powders on a nickel foil. As reference and counter electrodes were used Hg/HgO electrode and graphite rod, respectively. The specific capacitance C (F/g) at different current densities can be calculated via (1):

$$C = I \cdot \Delta t/m \cdot \Delta V, \tag{1}$$

where I (A) is a galvanostatic current, Δt (s) is the discharge time of a cycle, m (g) is the mass of the active material in the film electrode and ΔV (V) potential window. The mass of electroactive material of the working electrode was measured using a microbalance. The EIS were measured at a voltage amplitude of 5 mV in the frequency range between 50 kHz and 0.01 Hz.

3. Results and discussion

To determine the temperature of copper oxide formation from copper nitrate in the presence of glycine, thermogravimetry differential thermal analysis was performed on the basis of fully X-ray amorphous powder synthesized at $f = 0.05$ (Fig. 1). The obtained graph demonstrates that the main weight loss occurs in the temperature range from 90 to 370 °C and is accompanied by one endothermic peak (129 °C) and one exothermic peak (282 °C). The endothermic peak is explained by the process of decomposition of the initial crystal hydrate and removal of structured (crystalline) water, while the exothermic peak at 282 °C corresponds to the process of copper oxide formation and its crystallization and combustion of residual organic matter, which is in good agreement with previously published literature data [25, 26]. The absence of any additional exothermic effects above 300 °C allowed us to select this temperature for heat treatment of the samples to remove unreacted organics as described in the Experimental section.

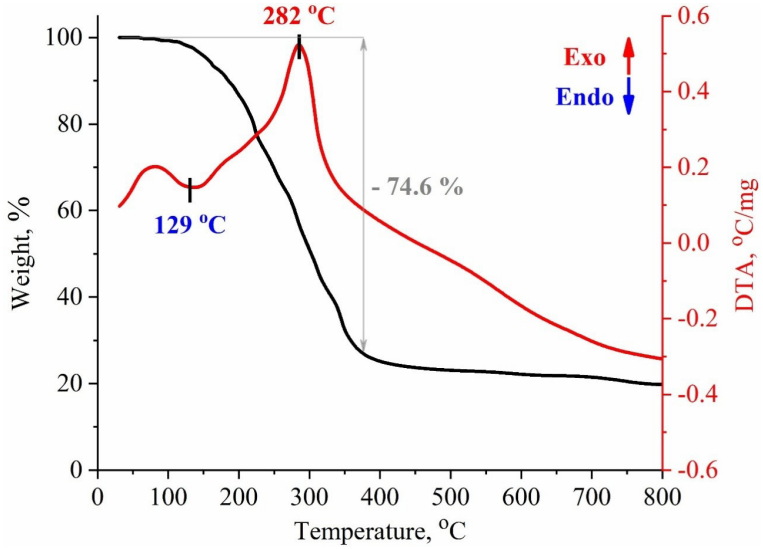

FIG. 1. DTA/TG curves of X-ray amorphous copper oxide powder synthesized with a significant lack of organic fuel ($f = 0.05$)

In order to establish the elemental composition and study the effect of the redox ratio on the morphology of the synthesized samples, micrographs and energy-dispersive spectra (Fig. 2) were obtained using scanning electron microscopy and energy-dispersive analysis. The data obtained indicate that all the synthesized compositions correspond in composition to copper oxide (CuO) within the error of the determination method (1 at. %). With an increase in f, the amount of copper and oxygen changes insignificantly, which indicates a stable ratio of the copper and oxygen content under all selected synthesis conditions. The presented micrographs showed that, regardless of the composition of the initial reaction solution, agglomerates consisting of nanoparticles are formed during the combustion process. It should be noted that the size of the agglomerates and the size of the particles increase significantly with an increase in the redox ratio f and are about 0.2 – 0.8 μm for the sample synthesized at $f = 0.2$ and 4 – 8 μm for the sample obtained at $f = 1.6$. With increasing parameter f, the structure becomes more porous, which follows from the increase in pore sizes in the micrographs. The sample obtained at $f = 0.2$ deserves special mention, since its morphology differs significantly from the previously published literature data. Thus, in work [23], the samples synthesized at glycine to nitrogen ratios in nitrates (G/N) equal to 0.3, 0.5 and 0.7 resemble the sample obtained at $f = 1.6$ in their morphology. However, compared to the samples synthesized at $f = 0.2$ and 1.0, the size of the agglomerates is significantly smaller and a different type of mesoporosity is visually observed in them, which can have a significant effect on the physicochemical behavior of copper oxide. It is well known that with a change in the fuel and oxidizer ratio, the temperature and intensity of combustion change, as a result of which the rate of nucleation and particle growth also changes. Higher temperatures and faster reactions can lead to the

formation of small particles due to rapid cooling and prevention of crystal growth, while slower reactions promote the formation of large particles and agglomerates (as shown in [23,27]). Due to the addition of nitric acid and the smoldering combustion mode in the case of a fuel shortage, it is possible to obtain submicron agglomerates that are several orders of magnitude smaller in size than in the case of using volumetric and surface combustion modes (stoichiometric ratio and excess of fuel).

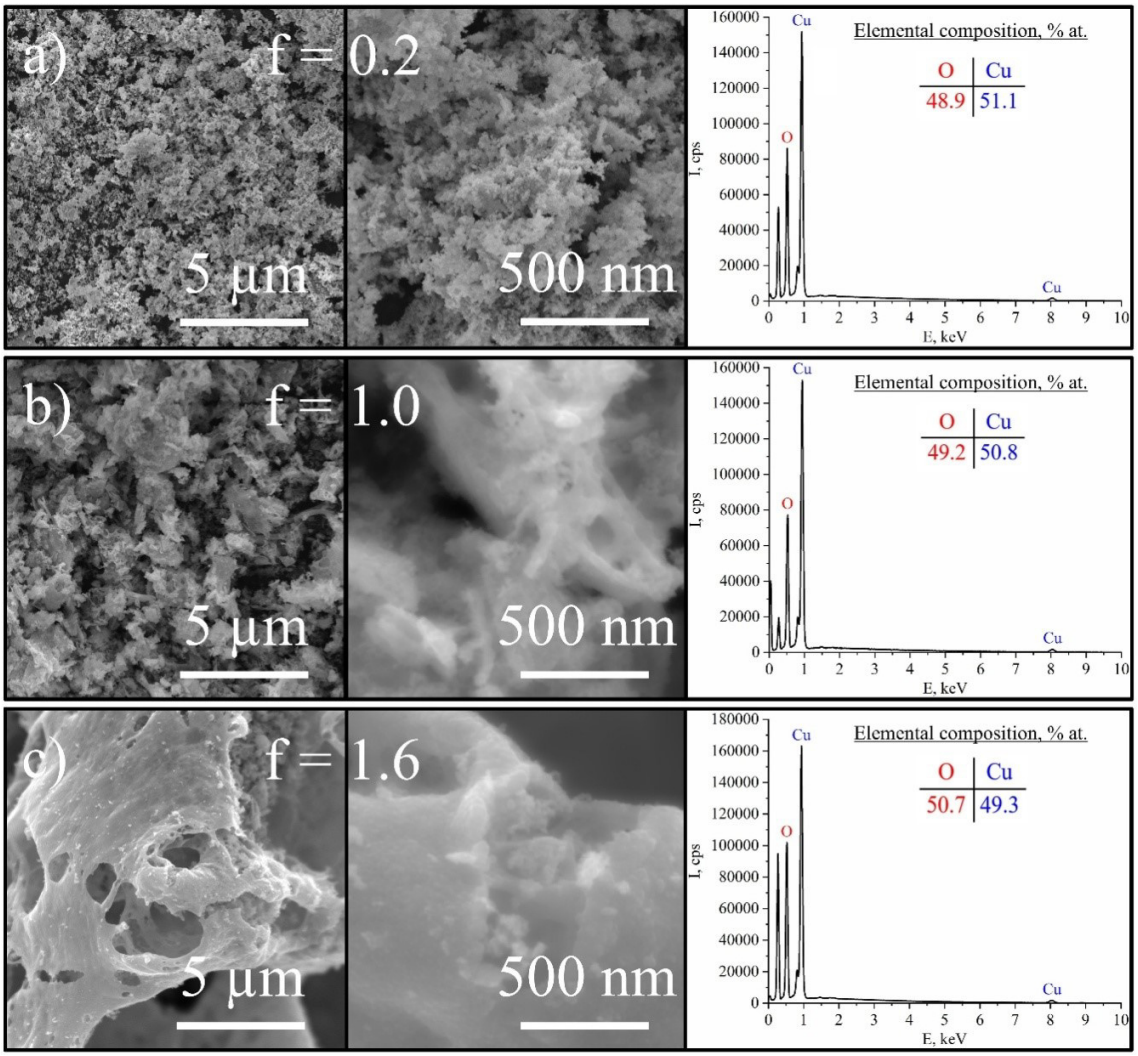

FIG. 2. Morphology and elemental composition of copper oxide nanopowders synthesized by solution combustion method at f ratios of 0.2 (a), 1.0 (b) and 1.6 (c)

To confirm the phase composition of the synthesized composites and conduct its structural analysis, they were studied by powder X-ray diffractometry, the results are shown in Fig. 3. According to the data obtained, the samples contain one crystalline phase – copper (II) oxide (ICDD No. 801916). The highest peak intensity is observed in the case of the sample synthesized at the stoichiometric redox ratio ($f = 1.0$), and in this sample the peaks have the smallest width. The absence of a shift in the diffraction maximum with respect to the reference card and the correspondence of the lattice parameters ($a = 4.684(1)$, $b = 3.422(1)$, $c = 5.143(2)$) to the literature data [28] allow us to assume that all samples are identical in terms of their crystalline structure. The lattice parameters are identical in all three samples, the difference appears only in the third digit. It should be noted that the samples obtained at $f = 0.2$ and 1.6 contain a significant proportion of the amorphous phase (36 and 21 %, respectively), which is caused by the low flame combustion temperature, which was insufficient for the final crystallization of the samples. The fraction of the crystalline phase for copper oxide synthesized at the stoichiometric ratio f is 6 %.

Figure 3(b) shows the crystallite distributions for all synthesized compositions. The center of gravity of the distribution constructed for the sample obtained at $f = 0.2$ is 4.8 nm, which indicates the presence of the smallest crystallites in this sample, with a fairly narrow distribution. With an increase in the redox ratio to stoichiometric ($f = 1.0$), the center of gravity of the distribution shifts to 18.6 nm, which is associated with an increase in the flame combustion temperature and a change in the combustion mode [29]. With a further increase in the amount of fuel in the reaction solution ($f = 1.6$), the crystallite size decreases to 10.7 nm, which is associated with a drop in the combustion temperature and a change in the

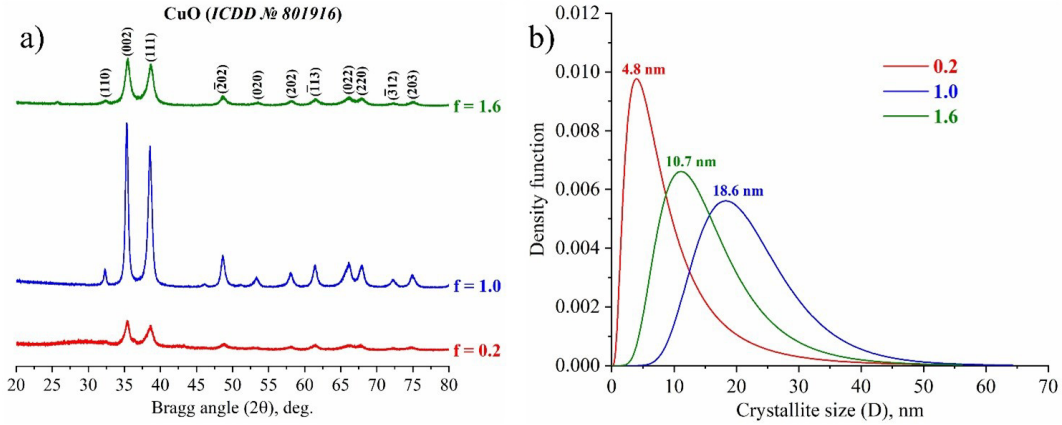

FIG. 3. Diffraction patterns (a) and crystallite size distribution (b) of copper oxide powders synthesized by solution combustion at different f ratios

combustion mode from bulk to surface. This behavior may be associated with more favorable crystallization conditions and, as a consequence, particle growth at higher f values.

Figure 4 shows the sorption-desorption isotherms of liquid nitrogen for copper (II) oxide samples synthesized under solution combustion conditions at different redox ratios f. All nanopowders demonstrate isotherms that have an appearance characteristic of type IV according to the IUPAC classification. The presence of hysteresis between the sorption and desorption branches in all samples confirms the mesoporous nature of the materials and the presence of capillary condensation. The sample synthesized at $f = 0.2$ demonstrated the highest volume absorption (up to 180 cm^3/g) at high relative pressures, which may indicate a more developed porous structure and a larger specific surface area (78.4 m^2/g). The samples synthesized at $f = 1.0$ and 1.6 have lower adsorption values, demonstrating lower porosity and a smaller specific surface area (14.4 and 22.3 m^2/g, respectively). It should be noted that in all three samples the greatest increase in adsorption occurs at relative pressures above 0.8, which also confirms the presence of large mesopores or macropores.

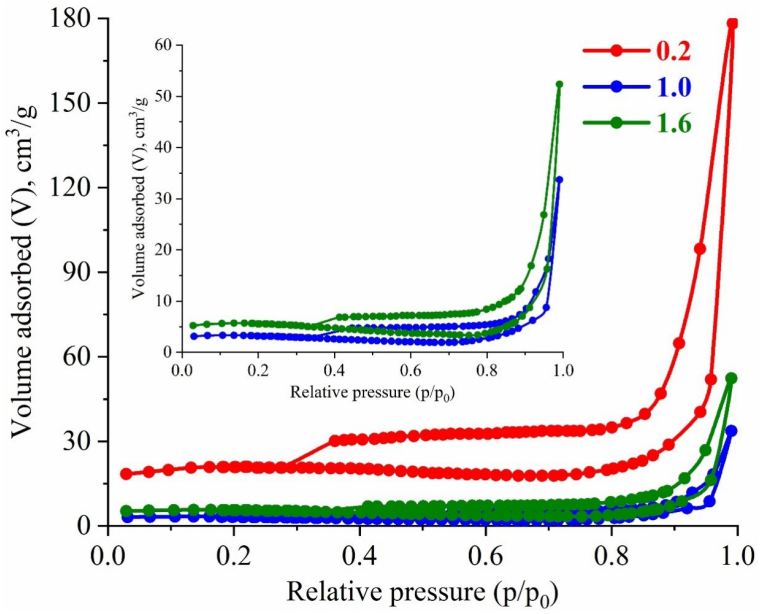

FIG. 4. N_2 adsorption-desorption isotherm (77 K) of the CuO nanopowders obtained at various f ratios

Cyclic voltammetry (CV) tests were conducted to assess the morphology-dependent electrochemical performance of CuO microstructures as active materials for supercapacitors. These measurements were carried out at a scan rate of 10 mV/s within a potential window of -0.2 to $+0.6$ V in a 1 M KOH aqueous electrolyte, as shown in Fig. 5. The CV curves of various microstructures exhibit pronounced redox peaks, indicating a reversible electron transfer process and the presence of a pseudocapacitive charge storage mechanism.

Extensive research has previously explored the electrochemical behavior of CuO nanostructures in alkaline electrolytes [13, 30]. The oxidation and reduction reactions of CuO in aqueous KOH occur within the potential range of 0 to 0.6 V. During the charging process, CuO undergoes reduction, resulting in cathodic peaks observed in the CV curves.

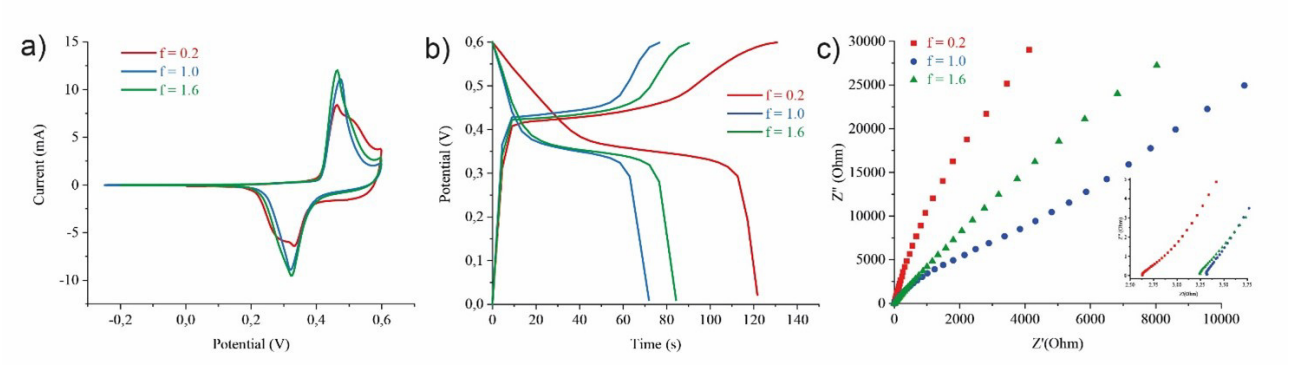

FIG. 5. CV (a) and GCD (b) curves; (c) Nyquist plots of of the CuO nanopowders obtained at various f ratios in 1 M KOH electrolyte

These cathodic peaks, illustrated in Fig. 5, correspond to the reduction of CuO/$Cu(OH)_2$ to Cu_2O/CuOH [13, 30]. The anodic peaks in the discharge cycle, presented in the CV curves (Fig. 5(a)), are attributed to the oxidation of Cu_2O/CuOH back to CuO/$Cu(OH)_2$ [30]. Consequently, the present CV data, in conjunction with earlier experimental findings, allows us to summarize the charging and discharging processes in the CuO electrode within this potential range with the following reactions [13]:

$$2\mathrm{CuO} + \mathrm{H_2O} + 2e^- \longleftrightarrow \mathrm{Cu_2O} + 2\mathrm{OH}^-,$$
$$\mathrm{Cu(OH)_2} + e^- \longleftrightarrow \mathrm{CuOH} + \mathrm{OH}^-.$$

The charge-discharge curves for the CuO samples in a 1 M aqueous KOH solution at a current density of 2 A/g are depicted in Fig. 5(b). These curves exhibit an asymmetric nature, highlighting the pseudocapacitive behavior of the CuO samples. The discharge curves reveal three distinct phases: an initial voltage drop linked to the internal resistance of the electrode, a linear potential variation over time indicative of double-layer capacitance due to charge separation at the electrode-electrolyte interface, and a slope variation over time reflecting the redox reaction between the electrolyte and the CuO electrode [12]. The specific capacitance was calculated from the galvanostatic discharge curves, with a comparative analysis showing that the CuO synthesized at $f = 0.2$ structure sustains a longer discharge time than both CuO synthesized at $f = 1.0$ and 1.6 respectively, underscoring the superior charge storage performance of the first microstructure. The specific capacitance values for CuO obtained at $f = 0.2$, cupper oxide synthesized at $f = 1.0$ and 1.6 were determined to be 405.5, 239.6, and 281.0 F/g, respectively.

The superior specific capacitance of the CuO synthesized at $f = 0.2$ microstructure is attributed to its high surface area and larger pore radius. Additionally, this sample possesses a greater pore volume, which facilitates the absorption of water molecules, acts as a buffering reservoir for ions participating in redox reactions, provides conductive pathways for enhanced interaction, and promotes rapid ion diffusion, thereby improving the kinetics of the reversible redox processes for charge storage. In contrast, the reduced specific capacitance observed in the other microstructures results from their lower surface area, smaller pore radius, and limited ion-exchange capabilities. Previous research has extensively investigated the charge-discharge profiles of CuO in pursuit of higher supercapacitance. Cycling stability is also a crucial parameter for evaluating supercapacitor performance; thus, the cycling stability of different microstructures was analyzed through galvanostatic discharge cycling (GDC) measurements at a rate of 2 A/g, as illustrated in Fig. 5(b).

Electrochemical impedance spectroscopy (EIS) measurements were performed to assess the charge kinetics of the device in relation to the aforementioned supercapacitive parameters. Fig. 5(c) presents the Nyquist plot of the CuO electrodes obtained through EIS, executed over a frequency range from 10 kHz to 0.05 Hz while maintaining open circuit potentials in a 1 M KOH electrolyte. Typically, the EIS spectra of supercapacitor electrodes can be deconvoluted into three segments, each corresponding to distinct processes [13]. First, the equivalent series resistance (ES) of the device can be evaluated at high frequencies. Next, capacitive behaviors are observed in the intermediate and low-frequency range. Finally, the Warburg diffusion region reflects the frequency-dependent ion diffusion and transport in the electrolyte at low frequencies. The high-frequency section of the EIS spectrum encompasses contributions from electrolyte resistance, the intrinsic resistance of the electroactive material, and the contact resistance between the active material and the current collector, all of which combine to represent the ES [30].

According to the equivalent circuit, the Nyquist plots were processed by the software and the calculated ES values were obtained. For the CuO electrodes examined, the values of R_s were determined to be 2.7, 3.3, and 3.3 Ω. This comparatively low resistance can be attributed to the one-dimensional morphology and enhanced crystallinity of the CuO electrodes. The EIS spectra revealed a small semicircle in the high-frequency region, indicative of the redox reactions occurring Cu^+/Cu^{2+} [13]. The diameter of this semicircle corresponds to the kinetic resistance to ion transfer, known as the charge transfer resistance (R_{ct}) associated with the redox processes. Notably, the calculated R_{ct} value for the

CuO synthesized at $f = 0.2$ sample was the lowest at 5.6 Ω (Table 1), which can be rationalized by the improved ionic conductivity and efficient diffusion of the electrolyte through the pores of the electrode material.

TABLE 1. The calculated R_{ct} and R_s value for the CuO synthesized at different f rations

	$f = 0.2$	$f = 1.0$	$f = 1.6$
R_s	2.7	3.3	3.3
R_{ct}	5.6	8.5	7.4·103

4. Conclusion

The use of the solution combustion method with glycine as an organic fuel allowed us to successfully synthesize copper oxide nanoparticles in the range from 4.8 to 18.6 nm with specific surface areas from 14.4 to 78.4 m^2/g. The smallest crystallite sizes and the largest specific surface area were observed for the sample synthesized with a significant fuel deficiency ($f = 0.2$). Chemical composition and phase analysis confirmed that all samples contained pure copper (II) oxide and its amorphous phase, the amount of which varied from 6 to 21 % depending on the reaction medium composition. All synthesized samples demonstrated pseudocapacitive behavior. The highest specific capacity values were observed for the sample obtained at the redox ratio $f = 0.2$, which is explained by the small crystallite size and its high specific surface area values.

References

[1] Guo T., Yao M.-S., Lin Y.-H., Nan C.-W., A comprehensive review on synthesis methods for transition-metal oxide nanostructures. *Cryst. Eng. Comm.*, 2015, **19** (17), P. 3551–3585.

[2] Sahoo S., Wickramathilaka K.Y., Njeri E., Silva D., Suib S.L. A review on transition metal oxides in catalysis. *Frontiers in Chemistry*, 2024, **12**, 1374878.

[3] Gaikwad P., Tiwari N., Kamat R., Mane S.M., Kulkarni S.B. A comprehensive review on the progress of transition metal oxides materials as a supercapacitor electrode. *Materials Science and Engineering: B*, 2024, **307**, 117544.

[4] Waris A., Din M., Ali A., Ali M., Afridi S., Baset A., Khan A.U. A comprehensive review of green synthesis of copper oxide nanoparticles and their diverse biomedical applications. *Inorganic Chemistry Communications*, 2021, **123**, 108369.

[5] Baranov O., Bazaka K., Belmonte T., Riccardi C., Roman H.E., Mohandas M., Xu S., Cvelbar U., Levchenko I. Recent innovations in the technology and applications of low-dimensional CuO nanostructures for sensing, energy and catalysis. *Nanoscale Horizons*, 2023, **8**, P. 568–602.

[6] Paul M.J., Suresh R., Akila T., Balasubramani V., Muthusamy S., Alarifi S., Ayub R. Standardizing the optimal photo-diode performance of CuO nanostructures through various morphological patterns. *J. of Alloys and Compounds*, 2024, **1000**, 175092.

[7] Poreddy R., Engelbrekt C., Riisager A. Copper oxide as efficient catalyst for oxidative dehydrogenation of alcohols with air. *Catalysis Science & Technology*, 2015, **4** (5), P. 2467–2477.

[8] Asamoah R.B., Annan E., Mensah B., Nbelayim P., Apalangya V., Onwona-Agyeman B., Yaya A. A Comparative Study of Antibacterial Activity of CuO/Ag and ZnO/Ag Nanocomposites. *Advances in Materials Science and Engineering*, 2020, **2020**, 7814323.

[9] Wang P., Gou X.-X., Xin S., Cao F.-F. Facile synthesis of CuO nanochains as high-rate anode materials for lithium-ion batteries. *New Journal of Chemistry*, 2019, **17** (43), P. 6535–6539.

[10] Doring G., Sternemann C., Kaprolat A., Mattila A., Hamalainen K., Schulke W. Shake-up valence excitations in by resonant inelastic x-ray scattering. *Physical Review B*, 2004, **70**, 085115.

[11] Dhineshbabu N.R., Rajendran V., Nithyavathy N., Vetumperumal R. Study of structural and optical properties of cupric oxide nanoparticles. *Applied Nanoscience*, 2016, **6**, P. 933–939.

[12] Gund G.S., Dubal D.P., Dhawale D.S., Shinde S.S., Lokhande C.D. Porous CuO nanosheet clusters prepared by a surfactant assisted hydrothermal method for high performance supercapacitors. *RSC Advances*, 2013, **46** (3), P. 24099–24107.

[13] Vidhyadharan B., Misnon I.I., Aziz R.A., Padmasree K.P., Yusoff M.M., Jose R. Superior supercapacitive performance in electrospun copper oxide nanowire electrodes. *J. of Materials Chemistry A*, 2014, **18** (2), P. 6578–6588.

[14] Li J., Mayer J.W. Oxidation and reduction of copper oxide thin films. *Materials Chemistry and Physics*, 1992, **32**, P. 1–24.

[15] Kim D.-S., Lee G.-H., Lee S., Kim J.-C., Lee H.J., Kim B.-K., Kim D.-W. Electrocatalytic performance of CuO/graphene nanocomposites for Li-O_2 batteries. *J. of Alloys and Compounds*, 2017, **707**, P. 275–280.

[16] Sonia S., Poongodi S., Kumar P.S., Mangalaraj D., Ponpandian N. Hydrothermal synthesis of highly stable CuO nanostructures for efficient photocatalytic degradation of organic dyes. *Materials Science in Semiconductor Processing*, 2015, **30**, P. 585–591.

[17] Christy A.J., Nehru L.C., Umadevi M. A novel combustion method to prepare CuO nanorods and its antimicrobial and photocatalytic activities. *Powder Technology*, 2013, **235**, P. 783–786.

[18] Mousali E., Zanjanchi M.A. Electrochemical synthesis of copper(II) oxide nanorods and their application in photocatalytic reactions. *J. of Solid State Electrochemistry*, 2019, **23**, P. 925–935.

[19] Saleem M.H., Ejaz U., Vithanage M., Bolan N., Soddique K.H.M. Synthesis, characterization, and advanced sustainable applications of copper oxide nanoparticles: a review. *Clean Technologies and Environmental Policy*, 2024, **6**, 02774.

[20] Varma A., Mukasyan A.S., Rogachev A.S., Manukyan K.V. Solution combustion synthesis of nanoscale materials. *Chemical Reviews*, 2016, **116** (23), P. 14493–14586.

[21] Martinson K.D., Kondrashkova I.S., Chebanenko M.I., Kiselev A.S., Kiseleva T.Yu., Popkov V.I. Morphology, structure and magnetic behavior of orthorhombic and hexagonal $HoFeO_3$ synthesized via solution combustion approach. *J. of Rare Earth*, 2022, **40** (2), P. 296–301.

[22] Patil S.P., Patil S.P., Puri V.R., Jadhav L.D. Synthesis and characterization of pure Cu and CuO nano particles by solution combustion synthesis. *AIP Conference Proceedings*, 2013, **1536** (1), P. 1260–1261.

[23] Cheng H.H., Chen S.-S., Liu H.-M., Jang H.-M., Chang S.-Y. Glycine–Nitrate Combustion Synthesis of Cu-Based Nanoparticles for NP9EO Degradation Applications. *Catalysts*, 2020, **10** (9), 1061.
[24] Dyachenko S.V., Martinson K.D., Cherepkova I.A., Zhernovoi A.I. Particle size, morphology, and properties of transition metal ferrospinels of the MFe_2O_4 (M = Co, Ni, Zn) type, produced by glycine-nitrate combustion. *Russian J. of Applied Chemistry*, 2016, **89**, P. 535–539.
[25] Murthy H.C.A., Zeleka T.D., Tan K.B., Ghotekar S., Alam M.W., Balachandran R., Chan K.-Y., Sanaulla P.F., Kumar M.R.A., Ravikumar C.R. Enhanced multifunctionality of CuO nanoparticles synthesized using aqueous leaf extract of Vernonia amygdalina plant. *Results in Chemistry*, 2021, **3**, 100141.
[26] Tamaekong N., Liewhiran C., Phanichphant S. Synthesis of Thermally Spherical CuO Nanoparticles. *J. of Nanomaterials*, 2014, **2014**, 507978.
[27] Sadabadi H., Aftabtalab A., Zafarian S., Chakra S., Venkateswara R., Shaker S. Influence of Fuel and Condition in Combustion Synthesis on Properties of Copper (II) Oxide Nanoparticle. *Advanced Materials Research*, 2013, **829**, P. 152–156.
[28] Su D., Xie X., Dou S., Wang G. CuO single crystal with exposed 001 facets – A highly efficient material for gas sensing and Li-ion battery applications. *Scientific Reports*, 2014, **4**, 5753.
[29] Martinson K.D., Murashkin A.A., Lobinsky A.A., Maltsev D.D., Qi K., Yu J., Almjasheva O.V., Popkov V.I. Structural, magnetic and electrochemical studies on $Zn_xMg_{1-x}Fe_2O_4$ nanoparticles prepared via solution combustion method. *Nanosystems: Physics, Chemistry, Mathematics*, 2024, **15** (2), P. 233–239.
[30] Kang M., Gewirth A.A. Voltammetric and Force Spectroscopic Examination of Oxide Formation on Cu(111) in Basic Solution. *The J. of Physical Chemistry B*, 2002, **106** (47), P. 12211–12220.

Submitted 10 December 2024; accepted 18 June 2025

Information about the authors:

Kirill D. Martinson – Ioffe Institute, Politekhnicheskaya st., 26, St. Petersburg, 194064, Russia; ORCID 0000-0001-9313-4267; martinsonkirill@mail.ru

Angelina O. Lebed – St. Petersburg Electrotechnical University "Leti", St. Petersburg, 199026, Russia; angelina.wdhs1@mail.ru

Hermann E. Litosov – St. Petersburg State Institute of Technology, 26 Moskovsky prospect, St. Petersburg, 190013, Russia; ORCID 0000-0001-7851-0148; xdutyx@yandex.ru

Maria V. Kaneva – Ioffe Institute, Politekhnicheskaya st., 26, St. Petersburg, 194064, Russia; ORCID 0000-0003-2816-7059; skt94@bk.ru

Artem A. Lobinsky – Ioffe Institute, Politekhnicheskaya st., 26, St. Petersburg, 194064, Russia; ORCID 0000-0001-5930-2087; lobinsky.a@gmail.com

Conflict of interest: the authors declare no conflict of interest.